performed on a i486DX2-66 MHz PC requiring computing time of 2.5 ms per unit cell and time step. On a 90 MHz P5, the computing time was 0.9 ms per unit cell and time step.

To validate the combination of SNM with ABC's, the S-parameters were computed for a symmetric open stub-type structure, which is shown in the inset of Fig. 2. The S_{21} parameter of the double stub is shown in Fig. 2, from which it can be seen that the data obtained with SNM is similar to data published in [10]. Both results, as well as the measured data, predict resonant frequencies at about 8 and 19 GHz. The structure in Fig. 2 was discretized into a $l \times m \times n = 18 \times 61 \times 80$ lattice, with $\Delta = 0.4$ mm. The total simulation time was $t = 9000 \times \Delta t$, where $\Delta t = 0.444$ ps. The S_{21} parameters show a good agreement near the first resonance. The SNM also appears to predict the value of S_{21} at the second resonant frequency with better accuracy than FDTD, when compared to the measured data.

Finally, the use of SNM is demonstrated for the analysis of a 3-D microstrip discontinuity. The multilayered substrate, shown in the inset of Fig. 3, is placed inside a waveguide with shielded side walls and open ends. The inner ends of the two microstrips are allowed to overlap or be slightly apart. The structure is discretized such that $l \times m \times n = 21 \times 21 \times 41$, with $\Delta = 0.5$ mm. For $\Delta t = 0.83$ ps, the total simulation time was $t = 1600 \times \Delta t$. The computed S_{11} and S_{21} parameters are shown in Figs. 3 and 4, respectively. Notice that as the ends of the lines are brought closer together, the magnitude S_{11} decreases, while that S_{21} increases. At higher frequencies, on the other hand, when the lines are tightly coupled, the magnitude of S_{21} is higher than that of S_{11}.

IV. Conclusion

The SNM algorithm was presented as a formal statement of the finite difference numerical scheme for the solution of Maxwell's equations. It was shown that the second-order ABC's can be employed in SNM for lattice truncation when dealing with open region problems. SNM is utilized in the study of planar and multilayered microstrip discontinuities. For the multilayered structure, it is shown that the effects of the overlap dimensions are very influential on the S-parameters. It is found that the SNM simulations can be effectively performed on a PC, yielding results comparable in accuracy to those obtained on lager computing platforms.

References

[1] R. H. Jansen, "The spectral domain approach for microwave integrated circuits," *IEEE Trans. Microwave Theory Tech.*, vol. MTT-33, pp. 1043–1056, Oct. 1985.

[2] S. Nam, H. Ling, and T. Itoh, "Characterization of microstrip line and its discontinuities using the time-domain method of lines," *IEEE Trans. Microwave Theory Tech.*, vol. 37, no. 12, pp. 2051–2057, Dec. 1989.

[3] T. Becks and I. Wolff, "Analysis of 3-D metallization structures by a full wave spectral domain technique," *IEEE Trans. Microwave Theory Tech.*, vol. 40, no. 12, pp. 2219–2227, Dec. 1992.

[4] H. Jin and R. Vahldieck, "The frequency-domain transmission line matrix method—A new concept," *IEEE Trans. Microwave Theory Tech.*, vol. 40, no. 12, pp. 2207–2218, Dec. 1992.

[5] X. Zhang and K. K. Mei, "Time-domain finite difference approach to the calculation of the frequency-dependent characteristics of microstrip discontinuities," *IEEE Trans. Microwave Theory Tech.*, vol. 36, no. 12, pp. 1775–1787, Dec. 1988.

[6] G. Mur, "Absorbing boundary conditions for the finite-difference approximation of the time-domain electromagnetic-field equations," *IEEE Trans. Electromag. Compat.*, vol. EMC-23, no. 4, pp. 377–382, Nov. 1981.

[7] R. L. Higdon, "Numerical absorbing boundary conditions for the wave equation," *Math. Computation*, vol. 49, no. 179, pp. 61–91, July 1987.

[8] R. Luebbers, "FDTD for antennas and scattering," in *Short Course Notes from 10th Annual ACES Conf.*, Monterey, CA, 1994.

[9] C. Eswarappa and W. J. R. Hoefer, "One-way equation absorbing boundary conditions for 3-D TLM analysis of planar and quasiplanar structures," *IEEE Trans. Microwave Theory Tech.*, vol. 42, no. 9, pp. 1669–1677, Sept. 1994.

[10] X. P. Lin and K. Naishdaham, "A simple technique for minimization of ABC-induced error in the FDTD analysis of microstrip discontinuities," *IEEE Microwave Guided Wave Lett.*, vol. 4, no. 12, pp. 402–404, Dec. 1994.

[11] N. Yoshida and I. Fukai, "Transient analysis of a stripline having a corner in three-dimensional space," *IEEE Trans. Microwave Theory Tech.*, vol. MTT-32, no. 5, pp. 491–498, May 1984.

[12] T. Shibata, T. Hayashi, and T. Kimura, "Analysis of microstrip circuits using three dimensional full wave electromagnetic field analysis in time domain," *IEEE Trans. Microwave Theory Tech.*, vol. 36, no. 6, pp. 1029–1035, June 1988.

[13] L. Lapidus and G. H. Pinder, *Numerical Solutions of Partial Differential Equations in Science and Engineering.* New York: Wiley, 1982.

Input Impedance of a Coaxial Probe Located Inside a Rectangular Cavity: Theory and Experiment

M. S. Leong, L. W. Li, P. S. Kooi, T. S. Yeo, and S. L. Ho

Abstract— **In this work, theoretical and experizmental analyzes of input impedance of a coaxial probe located in a rectangular cavity are presented. The technique of dyadic Green function (DGF) and the method of moments (MM) are applied in the theoretical analysis. For the magnetic equivalent source with a $\hat{y}$-directed discontinuity, two alternative representations of magnetic DGF for a rectangular cavity are derived in this paper. Numerical input reactance and phase of the reflection coefficient at the base of the probe obtained using both the conventional form and the alternative representations of the DGF are compared with the experimental data collected. It is found that the computed results obtained utilizing alternative DGF's agree better with the measured data.**

I. Introduction

The probe radiation inside a rectangular waveguide or cavity is an interesting and old problem. Since Schwinger studied the single-post problem during World War II for small posts, there have been many new advances on this problem. First, Collin [1, 1st ed.], early in 1960; Al-Hakkak in 1969 [2]; and Williamson [3], [4] from 1972 to 1985, used an important assumption that the current could be effectively represented by a filamentary current located at the center of the probe. In 1983 and 1984, Leviatan [5], [6] and in 1987, Jarem [7] used the eight equivalent current filaments representation to replace the conducting post surface and modified the previous single post with a central current. In 1991, Jarem [8] and in 1992 Liang *et al.* [9] included the effects from the frill current due to the probe located

Manuscript received June 11, 1995; revised March 20, 1996.

The authors are with the Department of Electrical Engineering, Communications and Microwave Division, National University of Singapore, Singapore 119260.

Publisher Item Identifier S 0018-9480(96)04723-0.

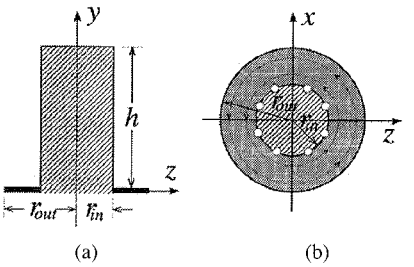

Fig. 1. (a) Side view and (b) top view of the excited probe. The equivalent surface current flowing circularly over the disk plate forms the magnetic source.

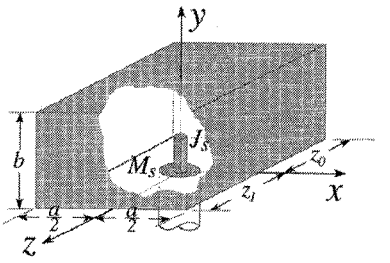

Fig. 2. Geometry of a rectangular cavity excited by a probe feed where the electric source is a line current distribution, and the equivalent magnetic source is a surface current distribution.

in the waveguide and cavity, and also derived the expression of the dyadic Green function (DGF's) in component form, respectively. Thus, for a probe considered (see Fig. 1), the eight equivalent current filaments form the electric current distribution $\boldsymbol{J}(\boldsymbol{r}')$ of $\hat{\boldsymbol{y}}$-direction and the equivalent current flow along the surface of the frill current aperture forms the magnetic current distribution $\boldsymbol{M}(\boldsymbol{r}')$ of both $\hat{\boldsymbol{x}}$- and $\hat{z}$-directions.

To calculate the input impedance of a probe in a rectangular cavity, an effective numerical implementation is usually to combine the DGF technique and the method of moments. For the electric source ($\hat{\boldsymbol{y}}$-directed) and the magnetic source ($\hat{\boldsymbol{x}}$- and $\hat{z}$-directed) (see Fig. 1), what one needs is only the $[\overline{\boldsymbol{G}}_e]_{yy}$-component of the electric DGF of the first kind, and the $[\nabla \times \overline{\boldsymbol{G}}_m]_{yx}$- and $[\nabla \times \overline{\boldsymbol{G}}_m]_{yz}$-components of the magnetic DGF of the second kind. The electric type of DGF for a rectangular cavity has been represented by Jarem [8] and Liang *et al.* [9] in components; and by Tai [10] and Li *et al.* [11], [12] in complete set. They also included the conventional form of magnetic DGF type with a step function along $\hat{z}$-direction. Minor corrections to the printing errors in [9] and numerical discussions were given by Li *et al.* in [13].

However, the equivalent magnetic source distributes over the frill current aperture on the $\hat{\boldsymbol{x}}\hat{z}$-plane. If the conventional representation of the magnetic DGF is substituted into the moment method procedure, the step function must be considered inside the double numerical integration throughout the entire range of evaluation. Theoretically, this can be improved if an alternative form of magnetic DGF for the $\hat{\boldsymbol{y}}$-directed discontinuity of the magnetic source is employed. It is found recently that the computational speed and accuracy can be increased if an alternative form of dyadic Green's functions is represented according to the source discontinuity. In the second section of this work, two alternative representations of magnetic DGF are derived taking the summation with respect to $\hat{\boldsymbol{y}}$-direction. The input reactance and phase of a reflection coefficient of the probe is computed using both the conventional form and the alternative representations of the electric type of DGF. Experimental results are presented and compared.

II. Electric Field and Method of Moments

The rectangular cavity configuration is shown in Fig. 2, where a, b, and $c = z_0 + z_1$ are the width, the height and the length, respectively.

This cavity is excited by a probe illustrated in Fig. 2. The probe feed is considered as an electric source while the current flow on the disk-shaped aperture is equivalent to a magnetic source. The side view (a) and the top view (b) of the probe are shown in Fig. 1. The electric current distribution is assumed to consist of eight uniform linear elements (see [7]). The magnetic equivalent current is assumed to flow circularly over the surface of the disk plate, as shown in Fig. 1.

In terms of these current distributions and the electric type of DGF's of the first and second kinds, the electric field is expressed as follows:

$$\boldsymbol{E}(\boldsymbol{r}) = -j\omega\mu \iiint_V \overline{\boldsymbol{G}}_e(\boldsymbol{r}, \boldsymbol{r}') \cdot \boldsymbol{J}(\boldsymbol{r}')\, dV' - \iiint_V \nabla \times \overline{\boldsymbol{G}}_m(\boldsymbol{r}, \boldsymbol{r}') \cdot \boldsymbol{M}(\boldsymbol{r}')\, dV'. \quad (1)$$

For this probe approximation, the electric source shown in Figs. 1 and 2 is assumed to have the $\hat{\boldsymbol{y}}$-component only and the magnetic source has the $\hat{\boldsymbol{x}}$- and $\hat{z}$-components. To calculate the input impedance of the probe, only the $\hat{\boldsymbol{y}}$-component of the electric field is needed [8], [9]. Thus, only three components of the DGF's, $[\overline{\boldsymbol{G}}_e]_{yy}$, $[\nabla \times \overline{\boldsymbol{G}}_m]_{yx}$ and $[\nabla \times \overline{\boldsymbol{G}}_m]_{yz}$, need to be derived.

The electric and magnetic current distributions in (1) are unknowns. To find out the unknown currents, the method of moment is applied. Expressing these current distributions in terms of a series of known basis (current flow) functions with unknown coefficients, we may express the field in terms of these unknown coefficients. The field over the surface of the probe must satisfy the boundary conditions, i.e., $E_{\tan} = 0$ on the surface of the probe. Therefore, the unknown coefficients can be solved numerically. Once the coefficients are obtained, the input impedance can then be calculated numerically, following the same procedure given by Jarem [7].

III. Alternative Representation of Magnetic DGF

A. The Conventional Form

The DGF's in (1) are assumed to be known. The electric DGF of the first kind was given by Tai [10] and the DGF's of both kinds represented by Li *et al.* [11] recently. The form is denoted as the $\hat{z}$-direction formula, but detailed expressions will not be given here. Using the complete electric type of DGF of the first kind $\overline{\boldsymbol{G}}_e(\boldsymbol{r}, \boldsymbol{r}')$ given by Tai [10] and that of the second type $\overline{\boldsymbol{G}}_m(\boldsymbol{r}, \boldsymbol{r}')$ provided by Li *et al.* [11], the input impedances of the probe with different locations are computed and compared with the measured data in Figs. 3 and 4.

B. The Alternative Form I

In principle, the field over the frill current aperture should not be affected by the step-functional change. However, the time for the above computation due to the step function is longer. To improve the computation, an alternative and appropriate representation of the DGF's is desirable. Since the discontinuity of the current distribution exists along the $\hat{\boldsymbol{y}}$-direction only, the step functional change

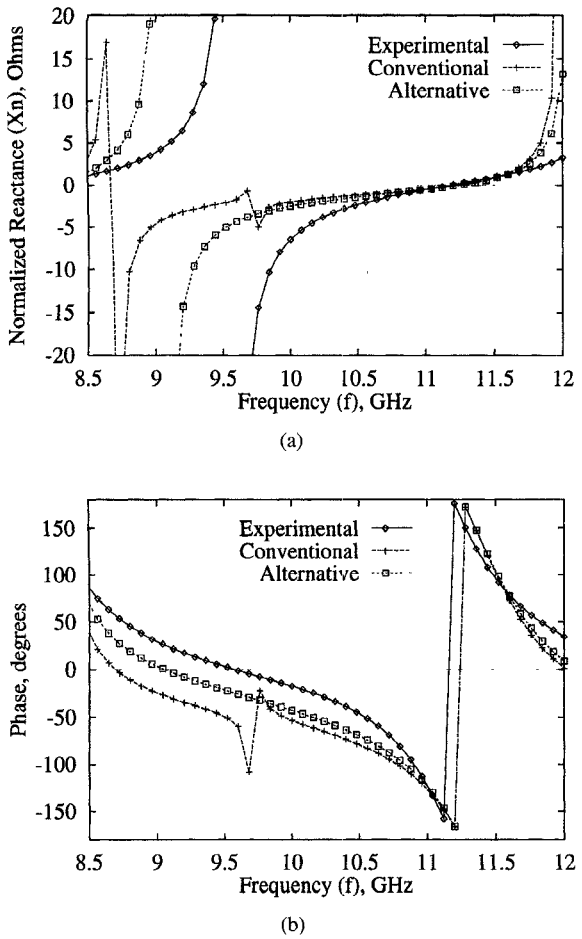

Fig. 3. Comparison of measured data denoted as "*experimental*" and numerical results computed using 1 the "*conventional*" DGF and 2 the "*alternative*" DGF, (a) reactance of the probe and (b) phase of a reflection coefficient. z-directed dimension c is 41.9 mm.

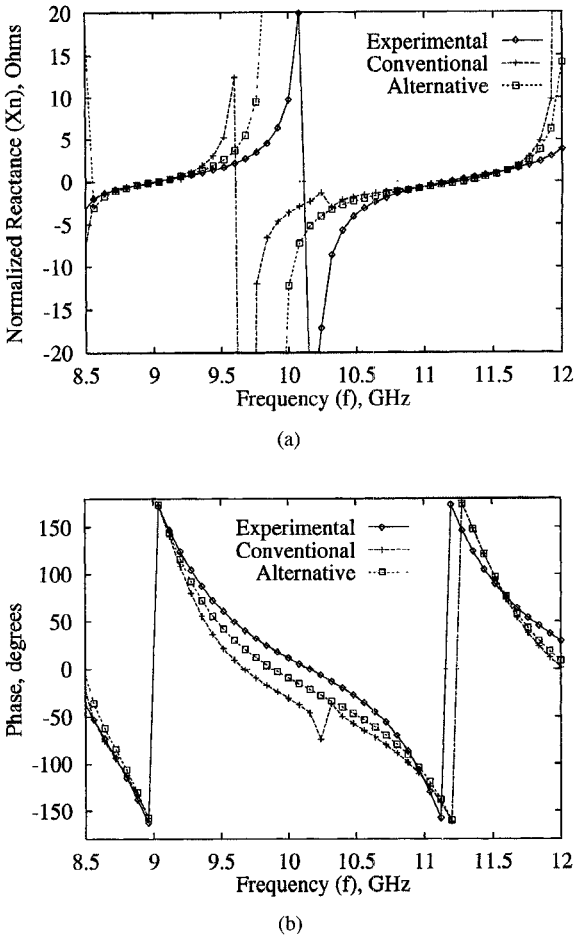

Fig. 4. The same as Fig. 3 except that z-directed dimension c is 56.9 mm.

along the $\hat{z}$-direction in the conventional form of DGF should be correspondingly alternated to that along the $\hat{\boldsymbol{y}}$-direction.

An alternative form of DGF for the rectangular cavity can be obtained by rotating the coordinate system and is given for $y \gtrless y'$ as follows:

$$\overline{\boldsymbol{G}}_m = -\frac{2}{ac}\sum_{mn}\frac{2-\delta_0}{k_c^2 k_g \sin(k_g b)}\begin{Bmatrix}\boldsymbol{M}^y_{omn}(b-y)\boldsymbol{M}'^y_{omn}(y') \\ \boldsymbol{M}^y_{omn}(y)\boldsymbol{M}'^y_{omn}(b-y')\end{Bmatrix} - \begin{Bmatrix}\boldsymbol{N}^y_{emn}(b-y)\boldsymbol{N}'^y_{emn}(y') \\ \boldsymbol{N}^y_{emn}(y)\boldsymbol{N}'^y_{emn}(b-y')\end{Bmatrix} \tag{2}$$

where the prime denotes the location (x', y', z') of the source, and the rectangular vector wave functions and the eigenvalues are given by

$$\boldsymbol{M}^y_{\substack{e\\o}mn}(y) = \nabla \times \left[\psi_{\substack{e\\o}mn}(x, y, z)\hat{\boldsymbol{y}}\right] \tag{3a}$$

$$\boldsymbol{N}^y_{\substack{e\\o}mn}(y) = \frac{1}{k}\nabla \times \nabla \times \left[\psi_{\substack{e\\o}mn}(x, y, z)\hat{\boldsymbol{y}}\right] \tag{3b}$$

and

$$k_x = \frac{m\pi}{a}$$
$$k_z = \frac{n\pi}{c} = \frac{n\pi}{z_0 + z_1} \tag{4a}$$

$$k_c = \sqrt{k_x^2 + k_z^2},$$
$$k_g = \sqrt{k^2 - (k_x^2 + k_z^2)} \tag{4b}$$

$$\psi_{\substack{e\\o}mn}(x, y, z) = \begin{bmatrix}\cos & \sin & \cos \\ (k_x x) & (k_g y) & (k_z z) \\ \sin & \cos & \sin\end{bmatrix}. \tag{4c}$$

C. The Alternative Form II

In addition to the above alternative form of DGF, another alternative form of DGF for the rectangular cavity can also be obtained by using the triple-summation form and summing the eigenvalues with respect to the $\hat{\boldsymbol{y}}$-direction. The second form is given for $y \gtrless y'$ as follows:

$$\overline{\boldsymbol{G}}_m = -\frac{2}{ac}\sum_{mn}\frac{2-\delta_0}{k_c'^2 k_g \sin(k_g b)}\begin{Bmatrix}\boldsymbol{M}_{omn}(b-y)\boldsymbol{M}'_{omn}(y') \\ \boldsymbol{M}_{omn}(y)\boldsymbol{M}'_{omn}(b-y')\end{Bmatrix} - \begin{Bmatrix}\boldsymbol{N}_{emn}(b-y)\boldsymbol{N}'_{emn}(y') \\ \boldsymbol{N}_{emn}(y)\boldsymbol{N}'_{emn}(b-y')\end{Bmatrix} \tag{5}$$

where the rectangular vector wave functions and the eigenvalues are given by

$$\boldsymbol{M}_{\substack{e\\o}mn}(y) = \nabla \times \left[\psi'_{\substack{e\\o}mn}(x, y, z)\hat{z}\right] \tag{6a}$$

$$\boldsymbol{N}_{\substack{e\\o}mn}(y) = \frac{1}{k}\nabla \times \nabla \times \left[\psi'_{\substack{e\\o}mn}(x, y, z)\hat{z}\right] \tag{6b}$$

and

$$k_x = \frac{m\pi}{a}$$
$$k_z = \frac{n\pi}{c} = \frac{n\pi}{z_0 + z_1} \tag{7a}$$

$$k_c' = \sqrt{k^2 - k_z^2}$$
$$k_g = \sqrt{k^2 - (k_x^2 + k_z^2)} \tag{7b}$$

$$\psi_{e_o mn}'(x, y, z) = \begin{bmatrix} \cos & \sin & \\ (k_x x) & (k_g y) & (k_z z) \\ \sin & \sin & \cos \end{bmatrix}. \tag{7c}$$

Using the above two alternative forms, the same mathematical expressions of $[\nabla \times \overline{G}_m]_{yx}$- and $[\nabla \times \overline{G}_m]_{yz}$-components of the magnetic DGF of the second kind can be found. Therefore, it will not be specified in the numerical results which alternative form has been implemented because the alternative forms provide the same formula used in the moment method.

For the frill current aperture in the $\hat{x}\hat{z}$-plane, the *step functional change* can be removed from the integral involving the components of the alternative magnetic DGF of the second kind because the integration is performed with respect to the elements dx and dz only. This property can be used *to increase the computational accuracy* as well *to speed up the computation* if the fast convergent forms of their respective components are used in the computation. The computed probe input reactances [Figs. 3(a) and 4(a)] and phases of the reflection coefficient [Figs. 3(b) and 4(b)] as seen at the base of the probe have been obtained and shown for different probe locations.

IV. Experiments

To show the validity of the two techniques using different forms of magnetic DGF, measurement is made in this work. The experimental data have been shown in Figs. 3 and 4 for cases I and II where the $\hat{z}$-directed dimension c is 41.9 and 56.9 mm, respectively. The dimensions of the rectangular cavity used in the experiment are: $a = 22.9$ mm, $b = 10.2$ mm, $c = z_1 + z_0 = 41.9$mm for case I and $c = z_1 + z_0 = 56.9$ mm for case II. As shown in Fig. 2, the probe with radius r_{in} of 0.65 mm and height h of eight.7 mm is located at the cavity center along the $\hat{x}$-direction, 31.9 mm far from the rear wall along the $\hat{z}$-direction for both case I and case II. The radius r_{out} of frill current aperture used in the measurement is 2.05 mm.

The experimental data are also compared with the computed results. The comparison has been shown in Figs. 3 and 4 for cases I and II. Reasonably good agreements between theory (using both the conventional and the alternative forms of the magnetic DGF's) and experiment, particularly at the frequency of interest ranging from 10–12 GHz, have been found, which demonstrates the applicability of the analyzes.

V. Concluding Remarks

In this work, we have presented theoretical and experimental analyzes of the input impedance of a probe located in a rectangular cavity. The method of moments and the DGF technique are applied in the computation of input impedance. Instead of the conventional representation of the DGF for the rectangular cavity published elsewhere, two alternative forms of the magnetic DGF of the second kind derived in this paper have been used in the numerical implementation. Experiment has been performed to examine the validity of these theoretical analyzes.

It has been found in this paper that the same formula of the DGF components, $[\nabla \times \overline{G}_m]_{yx}$ and $[\nabla \times \overline{G}_m]_{yz}$, are derived for the specified magnetic sources using the two alternative forms of magnetic DGF, and that the use of the alternative forms provides better computational accuracy of the input impedance compared with measured data. The computed results obtained using different methods show that a few kinks exist due to the poor convergence of the double integrals using standard IMSL routines on the plotted curves given using the conventional DGF form while a smooth curve is plotted using the alternative DGF representation. Comparison of the experimental data to numerical results illustrates that better agreement between the experimental data and the predicted results can be achieved if the alternative representation of the magnetic DGF is used in the (moment-method) computation.

References

[1] R. E. Collin, *Field Theory of Guided Waves,* 2nd ed. Piscataway, NJ: IEEE Press, 1991.

[2] M J. Al-Hakkak, "Experimental investigation of the input-impedance characteristics of an antenna in a rectangular waveguide," *Electron. Lett.*, vol 5, no 21, pp 513–514, 1969.

[3] A G. Williamson and D. V Otto, "Cylindrical antenna in a rectangular waveguide driven from a coaxial line," *Electron. Lett.*, vol. 8, no. 22, pp. 545–547, 1972

[4] A. G. Williamson, "Coaxially fed hollow probe in a rectangular waveguide," *Proc. IEE,* vol. 132, pt H, pp 273–285, 1985

[5] Y. Leviatan, P. G Li, A. T. Adams, and J Perini, "Single-post inductive obstacle in rectangular waveguide," *IEEE Trans. Microwave Theory Tech*, vol. MTT-31, pp 806–812, 1983.

[6] Y Leviatan, D. Shau, and A. T. Adams, "Numerical study of the current distribution on a post in a rectangular waveguide," *IEEE Trans. Microwave Theory Tech.,* vol. MTT-32, pp. 1411–1415, 1984.

[7] J. M Jarem, "A multifilament method-of moments solution for the input impedance of a probe-excited semi-infinite waveguide," *IEEE Trans. Microwave Theory Tech.*, vol. MTT-35, pp. 14–19, 1987

[8] ——, "A method of moments analysis and a finite-difference time-domain analysis of a probe-sleeve fed rectangular waveguide cavity," *IEEE Trans. Microwave Theory Tech.*, vol. 39, pp. 444–451, 1991.

[9] J. F. Liang, H. C. Chang, and K. A. Zaki, "Coaxial probe modeling in waveguides and cavities," *IEEE Trans. Microwave Theory Tech.,* vol. 40, pp. 2172–2180, 1992.

[10] C. T. Tai, *Dyadic Green's Functions in Electromagnetic Theory,* 2nd ed. Piscataway, NJ: IEEE Press, 1994.

[11] L. W. Li, P. S. Kooi, M. S. Leong, T. S. Yeo, and S. L. Ho, "On the eigenfunction expansion of dyadic Green's functions in rectangular cavities and waveguides," *IEEE Trans. Microwave Theory Tech.*, vol. 43, no. 3, pp. 700–702, Mar. 1995.

[12] L. W. Li, P. S. Kooi, M. S. Leong, T. S. Yeo, and S. L. Ho, "Input impedance of a probe-excited semi-infinite rectangular waveguide with arbitrary multilayered loads: Part I–Dyadic Green's functions," *IEEE Trans. Microwave Theory Tech.*, vol. 43, no. 7, pt. A, pp. 1559–1566, July 1995

[13] L. W Li, S L. Ho, M. S. Leong, P. S. Kooi, and T. S. Yeo, "Comment on 'coaxial probe modeling in waveguides and cavities,' " *IEEE Trans. Microwave Theory Tech*, vol. 43, no 7, pp 1629–1630, July 1995